Higgs boson decay into a lepton pair and a photon: A roadmap to the discovery of $H \to Z\gamma$ and probes of new physics

Aliaksei Kachanovich,[1,*] Ulrich Nierste,[1,†] and Ivan Nišandžić[2,‡]

[1]*Institut für Theoretische Teilchenphysik (TTP), Karlsruher Institut für Technologie (KIT), 76131 Karlsruhe, Germany*

[2]*Ruđer Bošković Institute, Bijenička cesta 54, 10000, Zagreb, Croatia*

(Received 5 October 2021; accepted 13 December 2021; published 11 January 2022)

The decay $H \to \ell^+\ell^-\gamma$, $\ell = e, \mu$ receives contributions from $H \to Z[\to \ell^+\ell^-]\gamma$ and a nonresonant contribution, both of which are loop induced. We describe how one can separate these subprocesses in a gauge-independent way, define the decay rate $\Gamma(H \to Z\gamma)$, and extract the latter from differential $H \to \ell^+\ell^-\gamma$ branching ratios. For $\ell = \mu$, also the tree decay rate, which is driven by the muon Yukawa coupling, is important. We propose kinematic cuts optimized to separate the three contributions, paving the way to the milestone (i) discovery of $H \to Z\gamma$, (ii) discovery of $H \to \mu^+\mu^-\gamma|_{\text{tree}}$, and (iii) quantification of new physics in both the effective H-Z-γ and nonresonant H-ℓ^+-ℓ^--γ couplings.

DOI: 10.1103/PhysRevD.105.013007

I. INTRODUCTION

Currently, ATLAS and CMS have put substantial effort into the discovery of the decay $H \to Z\gamma$. However, this process is only well defined when the Z boson is taken on shell. If one includes the effect of a nonvanishing Z decay width Γ_Z by smearing the off-shell $H \to Z\gamma$ decay amplitude with a Breit-Wigner distribution, one finds an unphysical, gauge-dependent result [1]. If the Z boson is detected through its leptonic decay, $H \to Z\gamma$ is a subprocess of $H \to \ell^+\ell^-\gamma$. The one-loop diagrams contributing to the process $H \to \ell^+\ell^-\gamma$ can be divided into three classes, namely, diagrams with an off-shell Z boson (describing $H \to Z^*[\to \ell^+\ell^-]\gamma$), those with an off-shell photon (involving $H \to \gamma^*[\to \ell^+\ell^-]\gamma$), and box diagrams. The calculations of the $H \to \ell^+\ell^-\gamma$ decay amplitude in an arbitrary linear R_ξ gauge in Ref. [2] have revealed how the sum of all diagrams in each class depend on the gauge parameter ξ of the W boson. This dependence cancels in the final physical result after the summation of all contributions. Complete one-loop calculations of differential decay rates (and asymmetries) of $H \to \ell^+\ell^-\gamma$ in the Standard Model (SM) have been performed by several groups [1–5], and Ref. [2] contains a detailed comparison of the numerical results presented in these references.

Nevertheless, it is possible to define a gauge-independent resonant contribution which peaks near $s = M_Z^2$, where $\sqrt{s}$ is the invariant lepton mass. The remaining contribution to $H \to \ell^+\ell^-\gamma$ consisting of $H \to \gamma^*[\to \ell^+\ell^-]\gamma$, box diagrams, and the gauge-dependent off-peak pieces of $H \to Z^*[\to \ell^+\ell^-]\gamma$ are all nonresonant and can be experimentally distinguished from the resonant term of interest. Next, one can employ the narrow-width approximation (NWA) to relate the latter to the product of the decay rate $\Gamma(H \to Z\gamma)$ and the branching ratio $\text{BR}(Z \to \ell^+\ell^-)$. Thus, one arrives at a physical, experimentally accessible definition of $\Gamma(H \to Z\gamma)$. Then, ruling out $\Gamma(H \to Z\gamma) = 0$ at 5 standard deviations will constitute the desired discovery of this decay mode.[1] At several steps of this derivation (for instance, by modifying the NWA), one could change the definition of $\Gamma(H \to Z\gamma)$ by terms of order Γ_Z^2/M_Z^2 and arrive at equally valid yet different results. This feature is intrinsic to any decay into an unstable particle detected only through its decay products. In view of the smallness of $\Gamma_Z^2/M_Z^2 \sim 10^{-3}$, however, this ambiguity is phenomenologically irrelevant.

The differential decay rate $d\Gamma(H \to \mu^+\mu^-\gamma)/dm_{\mu\mu}$ peaks at the photon and Z poles at $m_{\mu\mu} = 0$ and $m_{\mu\mu} \simeq M_Z$, respectively, and rises toward the end of the spectrum at $m_{\mu\mu} = M_H$ [see Fig. 2(b)]. The latter effect is due to the tree-level contribution involving the small muon Yukawa

*aliaksei.kachanovich@kit.edu
†ulrich.nierste@kit.edu
‡ivan.nisandzic@irb.hr

[1] t-$\bar{t}$-associated Higgs production has been recently proposed [6] as a particularly promising channel for the discovery of $H \to Z\gamma$ at the high-luminosity LHC.

coupling. ATLAS has already found evidence for $H \to \ell^+\ell^-\gamma$ in the low-invariant-mass region dominated by the photon pole [7]. To discover $H \to Z\gamma$, one must study the complementary region and in the $H \to \mu^+\mu^-\gamma$ data carefully separate the Z peak from $H \to \mu^+\mu^-\gamma|_{\text{tree}}$. A discovery of the latter contribution will constitute a manifestation of the Higgs Yukawa coupling to muons, independent of and complementary to the observation of $H \to \mu^+\mu^-$. The loop contribution to the decay rate of $H \to e^+e^-\gamma$ is several orders of magnitude larger than the corresponding tree contribution, as the latter is suppressed by the square of the tiny electron Yukawa coupling. We do not consider the process $H \to \tau^+\tau^-\gamma$ which is dominated by the tree-level contribution. The light lepton masses are neglected in the loop contributions which are found infrared finite in this limit.

With increasing statistics, one will be able to quantify deviations from the SM predictions not only for the effective H-Z-γ vertex, but also for the effective nonresonant H-ℓ^+-ℓ^--γ couplings. To this end, the data sample with $\ell = e$ and $\ell = \mu$ should not be combined, as new-physics (NP) contributions are likely to be different. Through the Higgs vacuum expectation value H-μ^+-μ^--γ, couplings can contribute to the anomalous magnetic moment of the muon, whose measurement significantly deviates from the SM prediction [8]. The nonresonant region between the photon and Z pole is best suited to probe those NP operators which are unrelated to the effective H-Z-γ vertex because the SM contribution is small.

This paper is organized as follows: In Sec. II, we separate the gauge-independent resonant contribution to $H \to \ell^+\ell^-\gamma$ related to the $H \to Z\gamma$ subprocess. Section III proposes various kinematic cuts to enhance the sensitivities to $H \to Z\gamma$, $H \to \mu^+\mu^-\gamma|_{\text{tree}}$, or nonresonant NP. In Sec. IV, we define $B(H \to Z\gamma)$ and relate this quantity to the resonant piece of $H \to \ell^+\ell^-\gamma$, and Sec. V presents the conclusions. Two Appendixes contain numerical input values and the loop function for $H \to Z\gamma$.

II. SEPARATING THE RESONANT CONTRIBUTION

We parametrize the loop-induced amplitude for the process $h \to \ell\ell\gamma$ as

$$\begin{aligned}\mathcal{A}_{\text{loop}} = &[(k_\mu p_{1\nu} - g_{\mu\nu} k\cdot p_1)\bar{u}(p_2)(a_1\gamma^\mu P_R + b_1\gamma^\mu P_L)v(p_1)\\ &+(k_\mu p_{2\nu} - g_{\mu\nu} k\cdot p_2)\bar{u}(p_2)\\ &\times(a_2\gamma^\mu P_R + b_2\gamma^\mu P_L)v(p_1)]\varepsilon^{\nu *}(k),\end{aligned} \tag{1}$$

where using the notation of Ref. [2], we denote the four-momenta of the photon, lepton, and antilepton by k, p_1, and p_2, respectively, while the chiral projectors are $P_{L,R} = (1 \mp \gamma_5)/2$.

The loop functions $a_{1,2}$ and $b_{1,2}$ depend on the Mandelstam variables

$$\begin{aligned}&s = (p_1 + p_2)^2, \qquad t = (p_1 + k)^2, \quad \text{and}\\ &u = (p_2 + k)^2 = m_H^2 + 2m_\ell^2 - s - t,\end{aligned} \tag{2}$$

where m_ℓ and m_H denote the masses of the lepton and Higgs boson. The coefficients a_2 and b_2 are obtained by exchanging the variables t and u within a_1 and b_1, respectively. Explicit one-loop expressions for the coefficients a_1 and b_1 can be found in Ref. [2] and corresponding ancillary files.

Each of the coefficients $a_{1,2}$ and $b_{1,2}$ can be written in the following form, e.g., for a_1:

$$a_1(s,t) = \tilde{a}_1(s,t) + \frac{\alpha_1(s)}{s - m_Z^2 + im_Z\Gamma_Z}, \tag{3}$$

with the obvious index replacement and the change of notation $\alpha_{1,2} \to \beta_{1,2}$ for the coefficients $b_{1,2}$. Note the relations

$$\alpha_1(s) = \alpha_2(s) \equiv \alpha(s) \quad \text{and} \quad \beta_1(s) = \beta_2(s) \equiv \beta(s). \tag{4}$$

As mentioned in the Introduction, the off-shell amplitude for $H \to \gamma Z^*$, which determines $\alpha(s)$ and $\beta(s)$, depends on the unphysical gauge parameter ξ. However, the process $H \to \gamma Z$ involving the on-shell Z boson does not depend on the gauge. Thus, we can isolate the ξ-independent part of the amplitude for the $H \to \gamma Z^*[\to \ell^+\ell^-]$ subprocess by setting $s = m_Z^2$ in $\alpha(s), \beta(s)$; i.e., the residue of the Z-boson propagator is gauge independent. In the following, we denote this term as the "resonant" contribution.

Separating the resonant and nonresonant terms in this way yields

$$a_1(s,t) = a_1^{nr}(s,t) + a_1^{\text{res}}(s), \tag{5}$$

$$\begin{aligned}a_1^{nr}(s) &\equiv \tilde{a}_1(s,t) + \frac{\alpha(s) - \alpha(m_Z^2)}{s - m_Z^2 + im_Z\Gamma_Z},\\ a_1^{\text{res}}(s) &\equiv \frac{\alpha(m_Z^2)}{s - m_Z^2 + im_Z\Gamma_Z}.\end{aligned} \tag{6}$$

We write

$$\frac{d^2\Gamma}{dsdt} = \frac{d^2\Gamma_{\text{loop}}}{dsdt} + \frac{d^2\Gamma_{\text{tree}}}{dsdt},$$

where the tree contribution in the second term is to be dropped for $\ell = e$. The loop contribution to the differential decay rate over the variables s and t is given by the formula

$$\frac{d^2\Gamma_{\rm loop}}{dsdt} = \frac{s}{512\pi^3 m_H^3}[t^2(|a_1|^2+|b_1|^2)+u^2(|a_2|^2+|b_2|^2)], \tag{7}$$

where we have neglected the light lepton masses in the phase space, and u is to be substituted for the expression in Eq. (2). The nonzero value of the lepton mass impacts the value of the loop-induced contribution to the decay rate only in the dilepton invariant-mass region close to the production threshold $m_{\ell\ell} \sim 2m_\ell$ via the kinematic effect. We avoid this region by using the cut $m_{\ell\ell,\rm min} \equiv \sqrt{\tilde{s}_{\rm min}} = 0.1 m_{\rm H}$ in what follows.

The square of the magnitude of a_1 in Eq. (6) contains three distinguishable pieces:

$$|a_1|^2 = |a_1^{nr}|^2 + |a_1^{\rm res}|^2 + 2{\rm Re}(a_1^{nr} a_1^{\rm res^*}), \tag{8}$$

and *mutatis mutandis* for a_2 and $b_{1,2}$. Corresponding contributions to the one-loop decay rate are

$$\frac{d^2\Gamma_{\rm loop}}{dsdt} = \frac{d^2\Gamma_{nr}}{dsdt} + \frac{d^2\Gamma_{\rm res}}{dsdt} + \frac{d^2\Gamma_{\rm int}}{dsdt}, \tag{9}$$

where the small interference term denoted by $\Gamma_{\rm int}$ corresponds to the third term in Eq. (8) and can be safely neglected for the purposes of expected near-future measurements.

The differential decay rate for the tree contribution for $H \to \mu^+\mu^-\gamma$ reads

$$\frac{d^2\Gamma_{\rm tree}}{dsdt} = \mathcal{N}\left[\frac{9m_\mu^4 + m_\mu^2(-2s+t-3u)+tu}{(t-m_\mu^2)^2} + \frac{9m_\mu^4 + m_\mu^2(-2s+u-3t)+tu}{(u-m_\mu^2)^2} + \frac{34m_\mu^4 - 2m_\mu^2(8s+5(t+u))+2(s+t)(s+u)}{(t-m_\mu^2)(u-m_\mu^2)}\right], \tag{10}$$

where

$$\mathcal{N} = \frac{e^4 m_\mu^2}{256\pi^3 \sin^2\theta_W m_W^2 m_H^3}. \tag{11}$$

For this distribution, we keep the nonvanishing muon mass in the formulas for physical kinematic limits given in Eq. (12). Note that the muon mass cannot be neglected in the phase space integral of the tree contribution; see Eq. (12) below.

The dependence of the loop and tree contributions to the differential decay rate on the Mandelstam variables s and t is displayed in the Dalitz plots in Fig. 1. With focus on the kinematic cuts required in the measurements, it is interesting to observe the behavior of the distributions in the endpoint regions of the Dalitz plots. While the one-loop contribution does not increase toward the boundaries, the tree distribution exhibits strong enhancements in the high-s, small-t, and small-u regions; see Eq. (10) above.

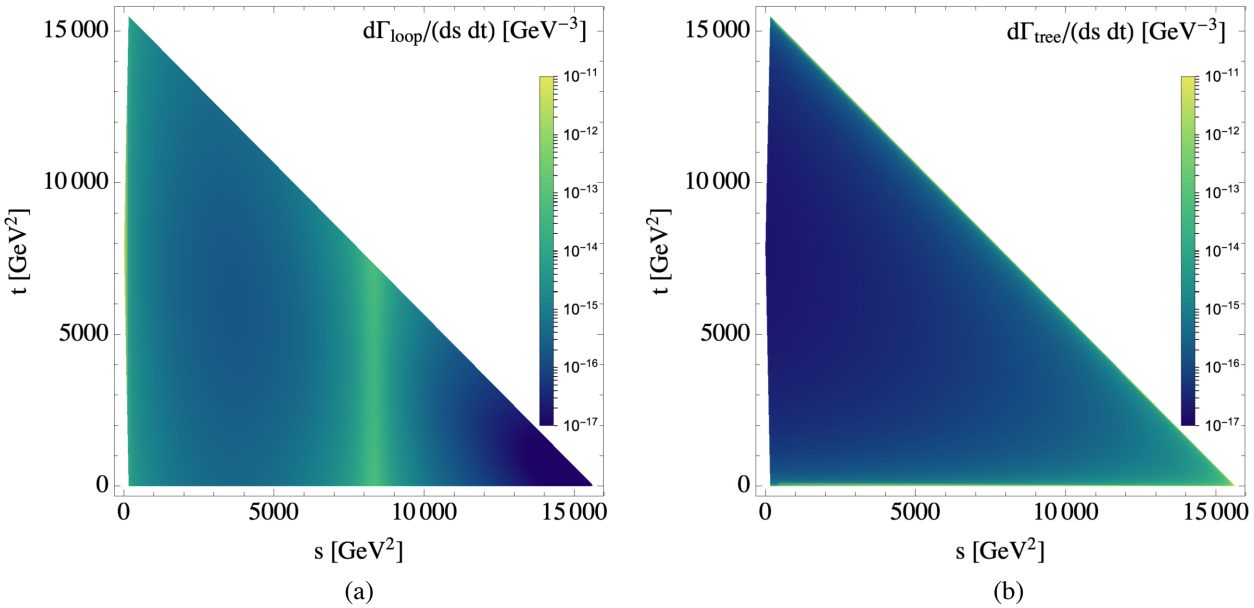

FIG. 1. Dalitz plot for (a) the one-loop contribution to the decay rate of $h \to \ell^+\ell^-\gamma$ and (b) the tree contribution to the decay rate of $h \to \mu\mu\gamma$.

With data on $\frac{d^2\Gamma}{dsdt}$, one can implement a very simple discovery strategy for $H \to Z\gamma$: Just insert $a_1^{\rm res}$ from Eq. (6) into Eq. (5) and the resulting expression for a_1 into Eq. (8) (and treat a_2 and $b_{1,2}$ in the same way), then use these results in Eq. (7), and finally add $\frac{d^2\Gamma_{\rm tree}}{dsdt}$. When using this formula to fit the three quantities $[\alpha(m_Z^2)]^2 + [\beta(m_Z^2)]^2$, $|a_1^{nr}|^2 + |b_1^{nr}|^2$, and $|a_2^{nr}|^2 + |b_2^{nr}|^2$ to the data, a 5σ signal of $[\alpha(m_Z^2)]^2 + [\beta(m_Z^2)]^2 \neq 0$ will imply the desired discovery. With Eq. (36) below, one can translate this measurement into a number for $\Gamma(H \to Z\gamma)$. Thus, after implementing the lengthy SM expressions for $a_{1,2}^{nr}$ and $b_{1,2}^{nr}$, one can directly compare $\Gamma(H \to Z\gamma)$ to the SM prediction in Eq. (30).

Next we discuss the various contributions to $\frac{d\Gamma}{dm_{\ell\ell}}$, where $m_{\ell\ell} = \sqrt{s}$ is the dilepton invariant mass. As a first step, we perform the integration over the full allowed range of the variable t, $t_{\rm min} \le t \le t_{\rm max}$ with

$$t_{\rm min(max)}(s, m_\ell) = \frac{1}{2}\Big(m_H^2 - s + 2m_\ell^2 \mp (m_H^2 - s)\sqrt{1 - 4m_\ell^2/s}\Big). \quad (12)$$

The resulting resonant and nonresonant one-loop distributions are shown in the left plot in Fig. 2. Since the masses of electrons and muons can be safely neglected in the one-loop calculation, Fig. 2(a) represents the loop correction for both cases. Furthermore, since the tree contribution for $H \to e^+e^-\gamma$ is negligible, $d\Gamma_{\rm loop}/dm_{\ell\ell}$ also represents the total contribution for $H \to e^+e^-\gamma$. The effect of the tree contribution is shown in Fig. 2(b). The only kinematic cut imposed for these plots is the one for the photon energy in the Higgs rest frame $E_{\gamma,\rm min} = 5$ GeV, which only lowers the maximum value of $m_{\ell\ell}$.

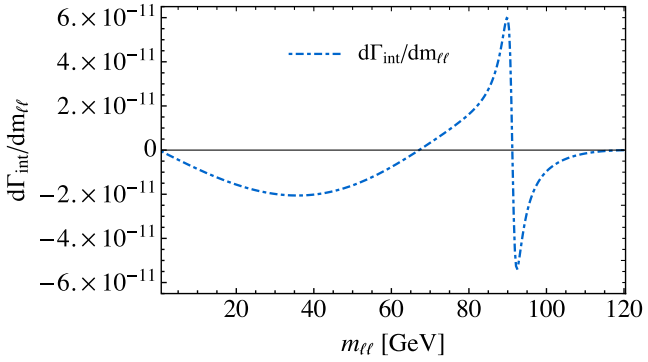

FIG. 3. Differential distribution $\frac{d\Gamma_{\rm int}}{dm_{\ell\ell}}$ with respect to invariant dilepton mass for $\ell = e, \mu$.

In Fig. 3, we display the interference contribution. As expected, this distribution changes sign at the value of $m_{\ell\ell}$ corresponding to the Z pole and is approximately symmetric around the null axis in this region. However, its magnitude turns out negligible within the full rate; this term is completely dropped in the following discussion.

III. KINEMATIC CUTS

In this section, we study the impacts of the kinematic cuts on the minimal values of the variables t and u on the resonant, nonresonant, and tree contributions.

We fix the kinematic range for the variable s all the way to Sec. III D as

$$\tilde{s}_{\rm min} = (0.1 m_H)^2, \quad \tilde{s}_{\rm max} = m_H^2 - 2m_H E_{\gamma,\rm min} = (120\,{\rm GeV})^2 \quad \text{with} \quad E_{\gamma,\rm min} = 5\,{\rm GeV}, \quad (13)$$

where $E_{\gamma,\rm min}$ the minimal photon energy in the rest frame of the Higgs boson.

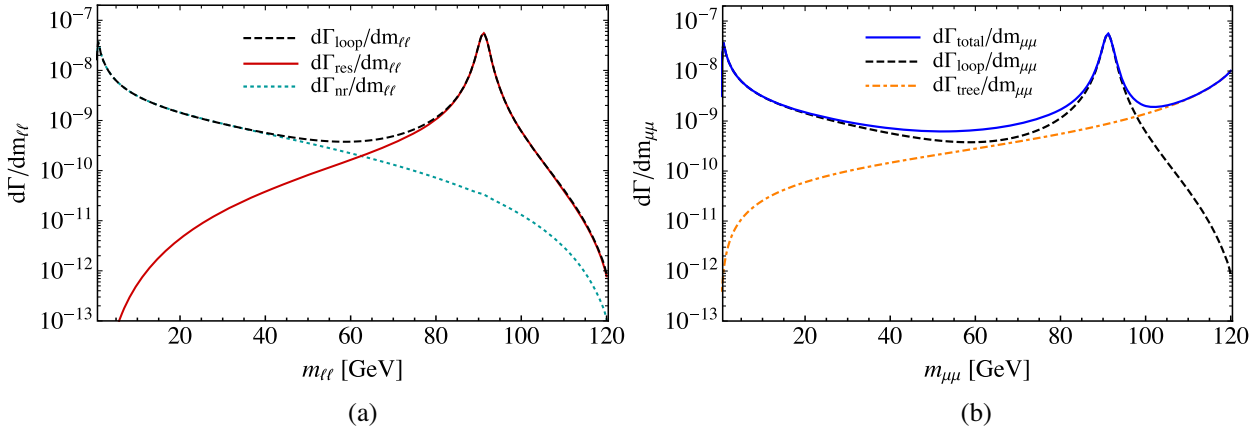

FIG. 2. One-loop contributions to differential decay rate with respect to the invariant dilepton mass for $\ell = e$ (a) and $\ell = \mu$ (b). The full one-loop, resonant and nonresonant contributions are denoted by black dashed, solid red, and turquoise dot-dashed curves, respectively. For the case $\ell = e$, the full one-loop contribution represents the full rate, while for $\ell = \mu$, the additional tree-level contribution needs to be accounted for.

The full physical range for the variable t is given in Eq. (12). We introduce the kinematic cuts on the minimal values of the t and u variables and denote them by $\tilde{t}_{\min} > 0$ and $\tilde{u}_{\min} > 0$. Note that the cut on the minimal value of variable u lowers the maximal value of t from the physical limit $t_{\max}(s)$ to $t_{\max}(s) - \tilde{u}_{\min}$.

Neither the resonant nor the nonresonant loop contribution exhibits a strong dependence on the small variations of the cuts on the t, u variables near the boundaries of the Dalitz plot; see Fig. 1(a) or Eq. (19) below. On the other hand, the tree contribution is peaking for the small values of t, as can be seen from the Dalitz plot boundary parallel to the s axis, and for the small values of u, as can be seen from the diagonal boundary of the plot in Fig. 1(b).

A. Resonant contribution

The resonant distribution is given by

$$\frac{d\Gamma_{\rm res}}{dsdt} = \frac{s(t^2+u^2)}{512 m_H^3 \pi^3} \frac{1}{(s-m_Z^2)^2 + m_Z^2 \Gamma_Z^2} (|\alpha(m_Z^2)|^2 + |\beta(m_Z^2)|^2), \tag{14}$$

with the mass of the light lepton neglected in the evaluations of both the kinematics and the a mplitude. With $m_\ell = 0$, the physical limits on the variable t are $t_{\min}(s) = 0$, $t_{\max}(s) = m_H^2 - s$, while $u = m_H^2 - s - t$. Numerical values of the loop coefficients at $s = m_Z^2$ are [2]

$$\alpha(m_Z^2) = -9.41 \times 10^{-6}\ \text{GeV}^{-1},$$
$$\beta(m_Z^2) = 1.17 \times 10^{-5}\ \text{GeV}^{-1}. \tag{15}$$

Integrating over the variable t, while imposing the cuts $\tilde{t}_{\min}$ and $\tilde{u}_{\min}$, we have

$$\frac{d\Gamma_{\rm res}}{ds}(s, \tilde{t}_{\min}, \tilde{u}_{\min}) = \frac{s}{512\pi^3 m_H^3} \frac{1}{(s-m_Z^2)^2 + m_Z^2 \Gamma_Z^2} (|\alpha(m_Z^2)|^2 + |\beta(m_Z^2)|^2) \cdot \left[\frac{t^3 + (s+t-m_H^2)^3}{3} \right]_{t=\tilde{t}_{\min}}^{t=\tilde{t}_{\max}=t_{\max}(s)-\tilde{u}_{\min}}. \tag{16}$$

A further integration over the variable s can also be performed analytically, but it results in a somewhat lengthy expression. In Fig. 4, we illustrate the variations of the resonant differential decay rate $d\Gamma_{\rm res}/dm_{\ell\ell}$ for different values of the cuts $(\tilde{t}_{\min}, \tilde{u}_{\min})$.

The effects of the cuts are more noticeable in the fully integrated decay rate. Integrating over s in the range given in Eq. (13), we have, e.g.,

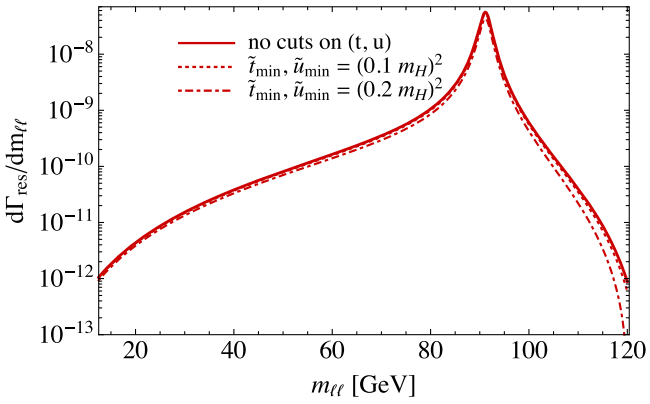

FIG. 4. The resonant decay rate distribution with respect to dilepton invariant mass $m_{\ell\ell}$ for different choices of the cuts $(\tilde{t}_{\min}, \tilde{u}_{\min})$.

$$\frac{\Gamma_{\rm res}[\tilde{t}_{\min} = (\kappa m_H)^2, \tilde{u}_{\min} = (\kappa m_H)^2]}{\Gamma_{\rm res}[\tilde{t}_{\min} = 0, \tilde{u}_{\min} = 0]} = (1, 0.94, 0.77) \quad \text{for } \kappa = (0, 0.1, 0.2) \tag{17}$$

with

$$\Gamma_{\rm res}[\tilde{t}_{\min} = 0, \tilde{u}_{\min} = 0] = 0.215\ \text{keV}. \tag{18}$$

B. Nonresonant contribution

The analytic form of the nonresonant contribution turns out rather lengthy; its explicit form can be read off from the expressions given in Appendix A of Ref. [2]. As in the previous case, we integrate the corresponding decay distribution over the variable t numerically from $\tilde{t}_{\min} > 0$ to the value $t_{\max}(s) - \tilde{u}_{\min} = m_H^2 - s - \tilde{u}_{\min}$. We illustrate the effect of several choices of the cuts $\tilde{t}_{\min}, \tilde{u}_{\min}$ on the nonresonant differential distribution over $m_{\ell\ell}$ in Fig. 5. Again, integrating over the variable s in the limits given in Eq. (13), we obtain

$$\frac{\Gamma_{nr}[\tilde{t}_{\min} = (\kappa m_H)^2, \tilde{u}_{\min} = (\kappa m_H)^2]}{\Gamma_{nr}[\tilde{t}_{\min} = 0, \tilde{u}_{\min} = 0]} = (1, 0.97, 0.87) \quad \text{for } \kappa = (0, 0.1, 0.2), \tag{19}$$

where

$$\Gamma_{nr}[\tilde{t}_{\min} = 0, \tilde{u}_{\min} = 0] = 0.043\ \text{keV}. \tag{20}$$

Therefore, we find weak dependence on the t, u cuts as long as the values of the latter are not such that they remove a significant amount of the phase space.

It is convenient to display the shapes of the distributions shown in Fig. 5 in an approximate numerical form. Since the dependence on the cuts is small, we represent the shape that does not involve any cuts on variables t, u as the following power series:

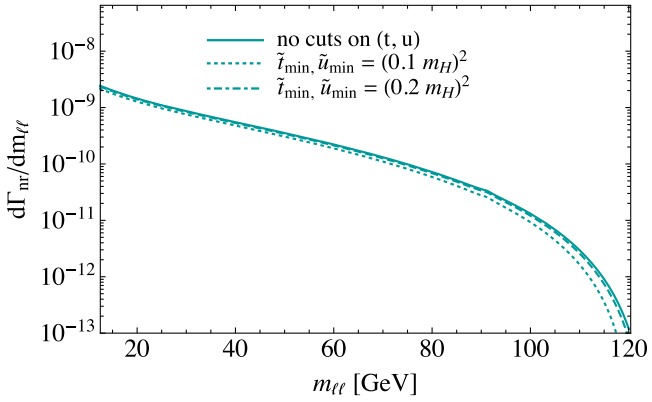

FIG. 5. The nonresonant decay distributions $d\Gamma_{nr}/dm_{\ell\ell}$ for few choices of the cut $\tilde{t}_{\min}$.

$$\frac{d\Gamma_{nr}}{dm_{\ell\ell}} = 10^{-10} \sum_{n=-4}^{3} c_n \left(\frac{m_{\ell\ell}}{m_H}\right)^n + \ldots \tag{21}$$

with

$$(c_{-4}, \ldots, c_3) = (3.27 \times 10^{-4}, -1.26 \times 10^{-2}, 2.0 \times 10^{-1}, 8.49 \times 10^{-1}, 7.96, -30.1, 32.1, -11.0). \tag{22}$$

The integral of the above approximate function over the variable $m_{\ell\ell}$ differs from the exact result at the level of around 0.5% (2%) for $m_{\ell\ell,\min} = 0.1 m_H$ $(0.5 m_H)$, with $m_{\ell\ell,\max} = 120$ GeV for both cases. This is an acceptable approximation given that the nonresonant part is itself a small contribution to the full decay rate in the interesting region around the Z-boson peak.

C. Tree contribution

The definite integral over the variable t in Eq. (10) can be performed analytically. As before, for the lower limit we have $\tilde{t}_{\min}$, which is larger than or equal to the physical lower limit $t_{\min}(s, m_\ell)$, while the upper limit is $t_{\max}(s, m_\ell) - \tilde{u}_{\min}$. Introducing the shorthand notation

$$\mathcal{I}(t) = \int dt \frac{d^2\Gamma_{\text{tree}}}{ds dt}, \qquad \mathcal{I}(a, b) \equiv \mathcal{I}(b) - \mathcal{I}(a), \tag{23}$$

the resulting distribution with respect to s is

$$\begin{aligned}\frac{d\Gamma_{\text{tree}}}{ds}(s; \tilde{t}_{\min}\tilde{u}_{\min}) &= \int_{\tilde{t}_{\min}}^{t_{\max}-\tilde{u}_{\min}} dt \frac{d^2\Gamma_{\text{tree}}}{ds dt}\theta(t - t_{\min}(s)) \\ &= \mathcal{I}(t_{\min}(s), t_{\max}(s) - \tilde{u}_{\min}) \\ &\quad - \theta(\tilde{t}_{\min} - t_{\min}(s))\mathcal{I}(t_{\min}(s), \tilde{t}_{\min}),\end{aligned} \tag{24}$$

where we have temporarily suppressed an additional dependence of $t_{\min(\max)}$ on the lepton mass for clarity of the notation. Note that the insertions of the Heaviside step function in the above equation confine the integration to the physically allowed region. The expression for $\mathcal{I}(t)$ is

$$\mathcal{I}(t) = \frac{\alpha^2 m_\ell^2}{16\pi m_H^3 m_W^2 \sin^2\theta_W}\left[\frac{2m_\ell^2(m_H^2 - 4m_\ell^2)}{t - m_\ell^2} + \frac{2m_\ell^2(m_H^2 - 4m_\ell^2)}{s + t - m_H^2 - m_\ell^2} - \frac{m_H^4 - 4m_H^2 m_\ell^2 + (s - 4m_\ell^2)^2}{s - m_H^2}\ln\left(\frac{s + t - m_H^2 - m_\ell^2}{t - m_\ell^2}\right)\right]. \tag{25}$$

The final formula for $\frac{d^2\Gamma_{\text{tree}}}{ds}(s; \tilde{t}_{\min}, \tilde{u}_{\min})$ is obtained by inserting the result of Eq. (25) into Eq. (24). We illustrate the dependence of the tree contribution on the cuts for several values of $\tilde{t}_{\min}$ and $\tilde{u}_{\min}$ in Fig. 6.

Finally, integrating over the variable s in the limits given in Eq. (13), we have

$$\frac{\Gamma_{\text{tree}}[\tilde{t}_{\min} = (\kappa m_H)^2, \tilde{u}_{\min} = (\kappa m_H)^2]}{\Gamma_{\text{tree}}[t_{\min}(s, m_\mu)]} = (1, 0.25, 0.12) \quad \text{for } \kappa = (0, 0.1, 0.2), \tag{26}$$

where

$$\Gamma_{\text{tree}}[\tilde{t}_{\min} = t_{\min}(s, m_\mu)] = 0.104 \text{ keV}. \tag{27}$$

D. Kinematic cuts and total rates

We now explore how each of the three contributions to the integrated decay rate depends on the cuts on variables

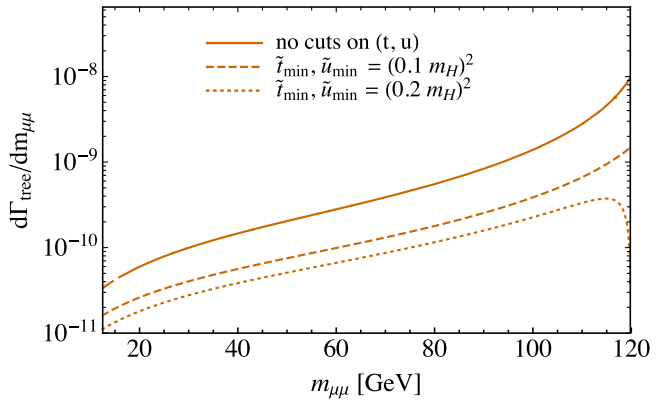

FIG. 6. Differential distribution $d\Gamma_{\text{tree}}/dm_{\mu\mu}$ with respect to invariant dimuon mass.

TABLE I. Integrated decay rates for different contributions to $H \to \mu^+\mu^-\gamma$ for several choices of the kinematic cuts on the variables s, t, and u. Note the symmetric choice $\tilde{u}_{\min} = \tilde{t}_{\min}$.

Cut	$s_{\min}$	$s_{\max}$	$\tilde{t}_{\min}, \tilde{u}_{\min}$	$\Gamma_{\rm res}$ (keV)	Γ_{nr} (keV)	$\Gamma_{\rm tree}$ (keV)	$\Gamma_{\rm tot}$ (keV)	Purpose
1	$(0.1m_H)^2$	$(120\ \text{GeV})^2$	$(0.1m_H)^2$	0.202	0.042	0.026	0.270	General
2	$(0.1m_H)^2$	$(120\ \text{GeV})^2$	$(0.2m_H)^2$	0.165	0.037	0.013	0.215	General
3	$(70\ \text{GeV})^2$	$(100\ \text{GeV})^2$	$(0.1m_H)^2$	0.195	0.002	0.007	0.204	$h \to Z\gamma$
4	$(70\ \text{GeV})^2$	$(100\ \text{GeV})^2$	$(0.2m_H)^2$	0.160	0.001	0.004	0.165	$h \to Z\gamma$
5	$(10\ \text{GeV})^2$	$(40\ \text{GeV})^2$	$(0.1m_H)^2$	3.53×10^{-4}	3.78×10^{-2}	1.02×10^{-3}	3.92×10^{-2}	Nonresonant
6	$(20\ \text{GeV})^2$	$(40\ \text{GeV})^2$	$(0.1m_H)^2$	3.33×10^{-4}	1.75×10^{-2}	8.12×10^{-4}	1.87×10^{-2}	Nonresonant
7	$(100\ \text{GeV})^2$	$(120\ \text{GeV})^2$	$(0.1m_H)^2$	1.93×10^{-3}	7.51×10^{-5}	1.5×10^{-2}	1.70×10^{-2}	Tree
8	$(100\ \text{GeV})^2$	$(120\ \text{GeV})^2$	$(0.2m_H)^2$	1.40×10^{-3}	5.28×10^{-5}	6.06×10^{-3}	7.51×10^{-3}	Tree

that also include s. We propose different cuts to optimize the sensitivity to the three milestones mentioned in the abstract. The results for several combinations of such cuts are shown in Table I.

Cuts 1 and 2 correspond to the choices of the three previous subsections.[2] For cut 1, we find that the nonresonant contribution is around 20% of the resonant one, while the tree contribution is somewhat larger than about 10%. As noted before, the tree contribution receives a strong suppression with the increasing values of $\tilde{t}_{\min}$ and $\tilde{u}_{\min}$. Cuts 3 and 4 isolate the resonant contribution stemming from $H \to Z\gamma$, while cuts 5 and 6 probe the nonresonant contribution. The purpose of cut 7 is the isolation of the tree contribution. Cut 8 simply illustrates an additional suppression of the tree contribution that results from tightening of cuts on t and u.

IV. RESONANT CONTRIBUTION AND THE NARROW-WIDTH APPROXIMATION

The resonant contribution is related to the decay rate of $H \to Z\gamma$ involving an on-shell Z boson that subsequently decays to a pair of light leptons.

We recall the amplitude for the process $H \to Z\gamma$:

$$\mathcal{A} = \tilde{\mathcal{A}}[(p_Z \cdot \epsilon(q)^*)(q \cdot \epsilon(p_Z)^*) - (p_Z \cdot q)(\epsilon(q)^* \cdot \epsilon(p_Z)^*)], \tag{28}$$

where p_Z, q, $\epsilon(p_Z)$, $\epsilon(q)$ denote the momenta and polarizations of the Z boson and photon, respectively, while the loop function $\tilde{\mathcal{A}}$ is given in Eq. (B1). The decay rate is

$$\Gamma(H \to Z\gamma) = \frac{(m_H^2 - m_Z^2)^3}{32\pi m_H^3} |\tilde{\mathcal{A}}|^2, \tag{29}$$

in agreement with the result in Ref. [9]. Evaluating $\tilde{\mathcal{A}}$ in Eq. (B1) for the input values of Eq. (A1) gives the SM prediction

$$\Gamma(H \to Z\gamma) = 6.51\ \text{keV}, \tag{30}$$

again in agreement with the numerical result found from the analytic expression in Ref. [9]. This value is 3% larger than the central value quoted by the LHC Higgs Cross Section Working Group, $\Gamma(H \to Z\gamma) = 6.31$ keV in Table 177 on page 679 of Ref. [10]; see also Eq. (III.1.18) on page 403. Reference [10] finds an uncertainty of the theory prediction of order 5%, which could be reduced by a two-loop calculation.

Furthermore, the branching ratio of the process $Z \to \ell\ell$ at tree level is

$$\text{BR}(Z \to \ell\ell) = \frac{m_Z}{\Gamma_Z}\tilde{C}, \qquad \tilde{C} = \frac{e^2(8\sin^4\theta_W - 4\sin^2\theta_W + 1)}{96\pi\cos^2\theta_W \sin^2\theta_W} \overset{\text{Eq.(A1)}}{=} 9.2 \times 10^{-4}. \tag{31}$$

Integration of the resonant distribution $d^2\Gamma_{\rm res}/(ds\,dt)$ over the variable t in the full range given in Eq. (12) results in

$$\frac{d\Gamma_{\rm res}}{ds} = \frac{s}{512\pi^3 m_H^3} \frac{1}{(s - m_Z^2)^2 + m_Z^2\Gamma_Z^2} \cdot \frac{2}{3}(m_H^2 - s)^3 \cdot (|\alpha(m_Z^2)|^2 + |\beta(m_Z^2)|^2). \tag{32}$$

We now apply the NWA for the Breit-Wigner distribution:

$$\text{NWA}: \frac{\Gamma_Z}{m_Z} \to 0, \quad \frac{1}{(s - m_Z^2)^2 + m_Z^2\Gamma_Z^2} \to \frac{\pi}{m_Z\Gamma_Z}\delta(s - m_Z^2), \tag{33}$$

where the limit is taken under the integral over s. Substituting this limit into Eq. (32), integrating this distribution over s, and using the relations (29) and (31) we find

$$\Gamma_{\rm NWA} = \Gamma(H \to Z\gamma) \cdot \text{BR}(Z \to \ell\ell), \tag{34}$$

provided that

[2]The upper limit on $s = (120\ \text{GeV})^2$ set for these two cuts is the result of imposing a minimal photon energy; see Eq. (13).

$$[\alpha(m_Z^2)]^2 + [\beta(m_Z^2)]^2 = 24\pi\tilde{\mathcal{A}}^2\tilde{C}. \tag{35}$$

The latter relation can be explicitly confirmed using the functions $\alpha(s)$ and $\beta(s)$ given in Eqs. (A.1) and (A.2) in Ref. [2]. Thus, if $[\alpha(m_Z^2)]^2 + [\beta(m_Z^2)]^2$ is extracted from the data, the desired decay width is calculated as

$$\Gamma(H \to Z\gamma) = \frac{(m_H^2 - m_Z^2)^3}{32\pi m_H^3}\frac{[\alpha(m_Z^2)]^2 + [\beta(m_Z^2)]^2}{24\pi\tilde{C}} \overset{\text{Eq.}(A1)}{=} (30.687\ \text{GeV})^3 \times [[\alpha(m_Z^2)]^2 + [\beta(m_Z^2)]^2] \tag{36}$$

with $\tilde{C}$ defined in Eq. (31).

Using Eq. (35), we can rewrite Eq. (16) as

$$\frac{d\Gamma_{\text{res}}}{ds}(s,\tilde{t}_{\text{min}},\tilde{u}_{\text{min}}) = \Gamma(H\to Z\gamma)\cdot \text{BR}(Z\to\ell\ell)\cdot\frac{3s\Gamma_Z}{2\pi m_Z(m_H^2-m_Z^2)^3}\cdot\frac{1}{(s-m_Z^2)^2+m_Z^2\Gamma_Z^2}\left[\frac{t^3+(s+t-m_H^2)^3}{3}\right]_{t=\tilde{t}_{\text{min}}}^{t=t_{\text{max}}(s)-\tilde{u}_{\text{min}}}. \tag{37}$$

The resulting decay rate is expressed as the function of the kinematic cuts $\tilde{t}_{\text{min}}$, $\tilde{u}_{\text{min}}$ and can be readily compared to the leading-order result for

$$\begin{aligned}\Gamma_{\text{NWA}} &= \Gamma(H \to Z\gamma)\cdot \text{BR}(Z \to \ell\ell) = 0.219\ \text{keV} \\ &= 0.0336 \times \Gamma(H \to Z\gamma)\end{aligned} \tag{38}$$

obtained using the parameter inputs from Eq. (A1).

V. CONCLUSIONS

The decay rate $\frac{d\Gamma(H\to\ell^+\ell^-\gamma)}{dm_{\ell\ell}}$ with $\ell = e$ or μ offers insights into different aspects of Higgs physics. With increasing integrated luminosity, it will be possible to (i) discover the decay $H \to Z\gamma$ and measure its branching ratio, (ii) discover the decay $H \to \mu^+\mu^-\gamma|_{\text{tree}}$ driven by the muon Yukawa coupling, and (iii) ultimately quantify potential new-physics contributions to both the loop-induced $H \to Z\gamma$ decay and the off-peak contributions to $H \to \ell^+\ell^-\gamma$. The latter comprise the nonresonant loop contributions, best tested in the region between the photon and Z poles, and (for $\ell = \mu$) $H \to \mu^+\mu^-\gamma|_{\text{tree}}$ which dominates $\frac{d\Gamma(H\to\ell^+\ell^-\gamma)}{dm_{\ell\ell}}$ near the end-point region with $m_{\ell\ell} > M_Z$.

In this paper, we have proposed a gauge-independent, physical definition of the decay rate $\Gamma(H \to \ell^+\ell^-\gamma)$ and shown how it can be extracted from the measured decay spectrum $\frac{d\Gamma(H\to\ell^+\ell^-\gamma)}{dm_{\ell\ell}}$. To this end, it is necessary to subtract the nonresonant contribution to $\frac{d\Gamma(H\to\ell^+\ell^-\gamma)}{dm_{\ell\ell}}$, and we have derived easy-to-use approximations for the cumbersome SM expression; see Eq. (21) above. We have further studied the dependence of $\frac{d\Gamma(H\to\ell^+\ell^-\gamma)}{dm_{\ell\ell}}$ on kinematical cuts, which we have only found to be a critical issue for $H \to \mu^+\mu^-\gamma|_{\text{tree}}$. In order to perform the three milestone measurements mentioned above, we have proposed cuts to optimize the sensitivities to $H \to Z\gamma$, $H \to \mu^+\mu^-\gamma|_{\text{tree}}$, and the nonresonant loop contribution, respectively; see Table I.

ACKNOWLEDGMENTS

A. K. and U. N. acknowledge support by DFG through CRC TRR 257, Particle Physics Phenomenology after the Higgs Discovery (Grant No. 396021762). I. N. would like to acknowledge support from the Alexander von Humboldt Foundation within the Research Group Linkage Programme funded by the German Federal Ministry of Education and Research.

APPENDIX A: INPUTS

We use the following values for the parameter inputs:

$$\begin{aligned} &m_W = 80.379\ \text{GeV}, \quad m_Z = 91.1876\ \text{GeV}, \quad \sin^2\theta_W = 1 - \frac{m_W^2}{m_Z^2} = 0.223013, \\ &m_t = 173.1\ \text{GeV}, \quad m_H = 125.1\ \text{GeV}, \quad m_\mu = 0.105658\ \text{GeV}, \quad \Gamma_Z = 2.4952\ \text{GeV}, \\ &G_F = 1.1663787 \times 10^{-5}\ \text{GeV}^{-2}, \quad \alpha^{-1} = \frac{\pi}{\sqrt{2}G_F m_W^2 \sin^2\theta_W} = 132.184. \end{aligned} \tag{A1}$$

APPENDIX B: THE LOOP FUNCTION $\tilde{\mathcal{A}}$

The loop function $\tilde{\mathcal{A}}$ introduced in Eq. (28) is given as

$$\begin{aligned}\tilde{\mathcal{A}} = \frac{e^3}{3\cdot 16\pi^2 \cos\theta_W \sin^2\theta_W m_W^2 (m_H^2 - m_Z^2)^2} \{&4(5 - 8\cos^2\theta_W) m_t^2 m_Z^2 m_W (B_0(m_H^2, m_t^2, m_t^2) - B_0(m_Z^2, m_t^2, m_t^2)) \\ &- 3 m_W m_Z^2 (2m_W^2 + m_H^2 - 12\cos^2\theta_W m_W^2 - 2\cos^2\theta_W m_H^2)(B_0(m_H^2, m_W^2, m_W^2) - B_0(m_Z^2, m_W^2, m_W^2)) \\ &+ m_W (m_Z^2 - m_H^2)(2(5 - 8\cos^2\theta_W) m_t^2 (m_H^2 - 4m_t^2 - m_Z^2) C_0(0, m_H^2, m_Z^2, m_t^2, m_t^2, m_t^2) \\ &- 6m_W^2 ((1 - 6\cos^2\theta_W) m_H^2 + 2(6\cos^4\theta_W + 3\cos^2\theta_W - 1) m_Z^2) C_0(0, m_H^2, m_Z^2, m_W^2, m_W^2, m_W^2) \\ &+ (3 - 6\cos^2\theta_W) m_H^2 + 4(8\cos^2\theta_W - 5) m_t^2 + 6(1 - 6\cos^2\theta_W) m_W^2)\}\end{aligned} \tag{B1}$$

expressed in terms of Veltman-Passarino loop functions [11] following the conventions of the FEYNCALC [12–14] package.

[1] G. Passarino, Phys. Lett. B **727**, 424 (2013).
[2] A. Kachanovich, U. Nierste, and I. Nišandžić, Phys. Rev. D **101**, 073003 (2020).
[3] A. Abbasabadi, D. Bowser-Chao, D. A. Dicus, and W. W. Repko, Phys. Rev. D **55**, 5647 (1997).
[4] D. A. Dicus and W. W. Repko, Phys. Rev. D **87**, 077301 (2013).
[5] T. Han and X. Wang, J. High Energy Phys. 10 (2017) 036.
[6] F. Goertz, E. Madge, P. Schwaller, and V. T. Tenorth, Phys. Rev. D **102**, 053004 (2020).
[7] G. Aad *et al.* (ATLAS Collaboration), Phys. Lett. B **819**, 136412 (2021).
[8] B. Abi *et al.* (Muon g-2 Collaboration), Phys. Rev. Lett. **126**, 141801 (2021).
[9] A. Djouadi, Phys. Rep. **457**, 1 (2008).
[10] D. de Florian *et al.* (LHC Higgs Cross Section Working Group), arXiv:1610.07922.
[11] G. Passarino and M. J. G. Veltman, Nucl. Phys. **B160**, 151 (1979).
[12] V. Shtabovenko, R. Mertig, and F. Orellana, Comput. Phys. Commun. **256**, 107478 (2020).
[13] V. Shtabovenko, R. Mertig, and F. Orellana, Comput. Phys. Commun. **207**, 432 (2016).
[14] R. Mertig, M. Bohm, and A. Denner, Comput. Phys. Commun. **64**, 345 (1991).